Efflux-linked Accelerated Evolution of Antibiotic Resistance at a Population Edge

Souvik Bhattacharyya[1*], Madhumita Bhattacharyya[2], Anjan K. Nandi[3], Dylan M. Pfannenstiel[1], YuneSahng Hwang[1], Khang Ho[1], and Rasika M. Harshey[1*]

Affiliations:

[1] Department of Molecular Biosciences and LaMontagne Center for Infectious Diseases, University of Texas at Austin; Austin, TX 78712

[2] Technical University of Munich, Augsburg, Germany

[3] Department of Physical Sciences, Indian Institute of Science Education & Research, Kolkata, India

*****Correspondence to either author: souvikut@utexas.edu; rasika@austin.utexas.edu

Abstract

How antibiotic-resistance mutations survive Darwinian forces in the absence of antibiotics is a long-standing question. We report an unexpected evolutionary phenomenon we call ‘phenotype surfing’ wherein twin phenotypes - high mutation frequencies and high efflux - segregate at the advancing edge of moving *E. coli* swarms. These phenotypes are linked: high efflux causes downregulation of specific DNA repair pathways, elevating mutations. We uncovered a genetic network connecting efflux and DNA repair, which we corroborated in a clinical 'resistome' database: genomes with mutations that increase efflux exhibit a significant increase in antibiotic-resistance mutations. Consequently, inhibitors that target efflux decreased evolvability to antibiotic resistance. Modeling shows how a mutator phenotype delivered to the edge by faster motility increases genetic drift, enabling survival and range expansion of mutants.

One Sentence Summary: A mutator phenotype resulting from high efflux 'surfs' to the edge of a moving *E. coli* swarm, where even unfit mutations survive and get fixed, as demonstrated for those conferring resistance to antibiotics.

Main Text

Genetic antibiotic resistance can evolve by Darwinian forces, where pre-existing mutations get positively selected when bacteria are exposed to antibiotics (*1*, *2*). In the absence of selection pressure, however, such mutations face elimination in two ways: first by genetic drift where such mutations can be randomly lost from the population (*3*, *4*), and second by a reduction in fitness. The latter is due to the essentiality of the cellular targets of antibiotics - transcription, translation,

or cell wall biogenesis – processes most often modified by the genetic resistance mechanisms (*5*). When competing with susceptible individuals in an antibiotic-free environment, mutations that confer resistance but alter cellular physiology will be disadvantageous (*6-8*). Compensatory mutations that rescue the reduced fitness of such mutants can arise (*9*), but could take a few tens of generations to appear (*10*), greatly increasing the chances of elimination of the original resistance mutation from the population (*8*). This has been demonstrated to be especially true when the density of population (and hence competition) is high (*11, 12*). We report here a phenomenon we call 'phenotype surfing', because of its resemblance to gene surfing (*13, 14*), where segregation of specific phenotypes at the edge of a dense mobile population allows even unfavorable mutations to survive.

Our model dense population is the *E. coli* swarm, where the bacteria move collectively over a semi-solid surface, powered by flagella (*15, 16*). Cells in a swarm grow and divide as they colonize ever-increasing swaths of territory; these cells are physiologically distinct from their planktonic counterparts. Unlike dense biofilms, in which bacteria have reduced metabolism and slow growth (*17, 18*), swarms are metabolically highly active (*19, 20*). An unexpected property of bacterial swarms is their tolerance to a broad class of antibiotics, which dissipates when the bacteria are removed from the swarm and dispersed in liquid (*21-23*). 'Tolerance' and 'persistence' are adaptive physiological mechanisms in bacteria that temporarily either turn down growth or turn up multidrug efflux pumps (*24*). Swarms exhibit elevated efflux and ROS catabolism and decreased membrane permeability even in the absence of antibiotic exposure, suggesting perhaps an anticipatory program to survive an encounter with antibiotics. ROS stress is known to be generated by high cell densities (*25, 26*) and by increased energy utilization expected during efflux (*27-29*). When confronted with antibiotics, swarms further elevate both

efflux and ROS catabolism. One of the proximate causes of this elevation is release of a 'necrosignal' from antibiotic-induced death of a sub-population. The antibiotic tolerance-enhancing factor was identified as being a part of an efflux pump itself: AcrA, a periplasmic component of the AcrAB-TolC RND efflux pump, is released from dead cells and signals live cells by interacting with TolC in the outer membrane to enhance drug efflux as well as to induce expression of many other efflux pumps (*30*). We have called this phenomenon 'necrosignaling' and have demonstrated its existence in other Gram-negative as well as Gram-positive bacteria (*30*).

We report here the convergence of several phenomena that create a high-evolvability niche at the advancing edge of an *E. coli* swarm. Cells at the edge are engaged in high efflux, likely for bringing in hard-to-get iron on a surface terrain. High efflux generates ROS stress, which may play a role in activating a genetic pathway that connects efflux to downregulation of specific DNA repair genes, producing a mutator phenotype. Motility plays another important role in assisting this phenotype to 'surf' to the edge of the swarm where genetic drift, and hence chances of fixation of unfit mutations, are expected to be high. Edge cells incur more cell death as well, releasing the necrosignal AcrA, which stimulates efflux further. We show that the mutator phenotype can be suppressed by inhibitors that target both AcrA and the efflux pump.

Results and Discussion

Swarms downregulate DNA repair and show high evolvability to antibiotic resistance

Compared to planktonic populations, *E. coli* swarms intrinsically upregulate efflux and ROS catabolism pathways (*30*). A study showing a correlation between increased efflux pump activity

and downregulation of the DNA repair gene *mutS* in planktonic cells of *E. coli* (*31*), led us at first to re-examine our *E. coli* RNA seq data from swarms, which showed a 3-6 fold downregulation of eight DNA repair genes – *dinB*, *holA*, *lexA*, *mug*, *mutM*, *mutS*, *recC*, and *ung* (Fig. 1A inset and fig. S1A). These genes are broadly involved in mismatch and nucleotide-excision repair, predicting a mutator phenotype. This was tested by examining for the presence of mutants resistant to the antibiotic Kanamycin (Kan^R) in the swarm, using a modification of the border-crossing assay originally designed to demonstrate antibiotic tolerance in swarms (*22*). *E. coli* can swarm collectively on the surface of media solidified with ~0.5% agar (videos S1, S2), but will swim as individuals within softer agar (0.3%) (*19*). Swimming bacteria are effectively in a planktonic state, so we will henceforth use S and P symbols to denote swarm and planktonic states. In the assay, a 2-chamber Petri dish filled with swarm media contains antibiotic in only one chamber; bacteria that begin swarming in the no-antibiotic chamber and arrive at the separating border, will attempt to cross over and colonize the antibiotic chamber. To detect individual bacteria harboring Kan^R mutations that arose within the swarm, we modified this assay to contain swim media with Kan in the right chamber (Fig. 1B schematic; S to P setup). A control set-up for observing such mutants arising in the P population had swim media in both chambers (P to P setup).

Kan^R mutants were recovered in both P-P and S-P set-ups (Fig. 1C-D). The distinct points along the border from where the Kan^R swim 'flares' emerge report on the physical location of the original mutant in the S or P population, which then colonizes the area on the right. Kan^R mutants were recovered at a higher frequency per plate in S-to-P compared to P-to-P setups (Fig. 1C-D and fig. S1B). A total of 32 Kan^R mutants were collected, 25 that arose from S-P setup, and 7 from the P-P setup. To determine the mutation frequency (MF) accurately, we measured

resistance to the antibiotics Rifampicin (Rif) and Kan (*32-34*) in both populations. Compared to P cells, S cells of *E. coli* exhibited a ~5-fold higher MF (Fig. 1E). To test if this was a general feature of S cells, MFs were also calculated for S cells of *Bacillus subtilis* (Fig. 1F) and *Pseudomonas aeruginosa* (fig. S1C), which showed ~8- and ~7-fold MF increases, respectively, compared to their P counterparts.

Differences in the intensity and size of the flares that emerged in the *E. coli* set up in Fig. 1C, could be indicative of differences in the proficiency of growth and/or motility of the mutants. We therefore examined these parameters closely in all 32 mutants, as well as identified the mutations by whole-genome sequencing. Mutants derived from P cells (P1-7) were uniformly poor in motility (M) (Fig. 1G), whereas those from S cells varied in this property, some moving even better than wild type (WT) (S1-25) (Fig. 1G and fig. S1D). P-derived mutants were also uniformly poor in growth (G) (Fig. 1G and fig. S1E), whereas S-derived mutants clustered into four distinct groups, some growing as well as WT (Fig. 1G and fig. S1E). DNA sequencing revealed an enrichment of mutations in three genes – *fusA*, *cydA*, *dgcJ* - across the mutant set (Fig. 1H). *fusA* encodes elongation factor G (EF-G), which is a known source of Kan^R mutants (*35*) as Kan inhibits translation by binding to the A site in the 30S ribosomal subunit, blocking EF-G catalyzed translocation. *cydA* encodes subunit I of cytochrome bd-I terminal oxidase. Kan^R mutations previously isolated in *cydA* (*36*) resulted in decreased PMF and were inferred to have decreased Kan uptake (*37*). The third gene *dgcJ* is a putative cyclic di-GMP synthase and has no reported connection to Kan^R, but is expected to increase motility (*38, 39*). To test if these mutations directly conferred the Kan^R phenotype, wild-type copies of all three genes were overexpressed in four representative isolates, yielding the following results. Overexpression of *fusA* caused Kan^R to diminish only in strains with *fusA* mutations (Fig. 1I, S1&S2 set; fig. S1F),

while *cydA* overexpression reduced Kan^R only in strains with *cydA* mutations (Fig. 1I, S6&S9 set; fig. S1F). Overexpression of *dgcJ* did not abrogate the Kan^R phenotype in strains with *dgcJ* mutations (Fig. 1I, S6&S9 set), but greatly reduced swimming motility of all strains tested, including that of WT (Fig. 1J, swim; fig. S1G), consistent with the known role of c-di-GMP (the enzymatic output of DgcJ) in inhibiting motility. In summary, these experiments confirm that mutations in *fusA* and *cydA* confer Kan^R, whereas DgcJ may have a specific role in swarming motility as indicated by the abundance of *dgcJ* mutants in isolates only from the S samples.

The relationship of *cydA*, *fusA* and *dgcJ* mutations in promoting Kan^R and motility is sketched Fig. 1K, based on literature reports. Mapping the mutations associated with the three genes onto the known or predicted structures of these three proteins showed that for EF-G, most mutations mapped to residues known to affect the translocation of the ribosome (*40*), but the two that map to domain I and II of EF-G, respectively (*41*), have no known connection with translocation (R146 and T393) (Fig. 1L). For CydA, the two mutants isolated were at positions not previously associated with Kan^R (*42*) (Fig. 1M). For DgcJ, four were in the predicted enzyme active site (*43*), while one (black) was mapped on the predicted sensory domain (Fig. 1N).

In summary, the results in this section show that *E. coli* swarms downregulate a set of eight specific DNA repair genes and expectedly, show higher MFs. This observation is not unique to *E. coli* swarms, as high MFs are also observed in *B. subtilis* and *P. aeruginosa* swarms. A large majority of Kan^R mutants recovered from edge of *E. coli* swarms are accompanied by mutations that improve their motility in the swarm.

Downregulation of mismatch and base excision repair pathways contributes to the higher MFs of swarm cells

A detailed analysis of all the mutations recovered in the genomes of the 32 mutants (Fig. 1G) revealed that of 501 total mutations identified, A→G and T→C changes were each ~5% lower in S compared to P isolates, whereas T→G and C→T changes were each ~2-3% higher in S (Fig. 2A and fig. S2A). Overall, transition mutations decreased by ~11% and transversions increased by ~8% in S isolates (Fig. 2B, whole genome). Considering only the mutations in genes conferring Kan^R – *fusA* and *cydA* – transitions decreased ~ 21% and transversions increased ~6% in S compared to P cells (Fig. 2B, Kan^R). Two other types of mutations isolated across the genome were indels. Of these, insertions ranging from 4 -11 bp were found in *dgcJ* whereas deletions from 6-9 bp were found in *cydA*. We found no bias in the distribution of mutations in coding or non-coding regions (Fig. 2B and fig. S2B).

To test which repair pathway might be responsible for the mutations recovered in S cells, these cells were exposed to mutagenic agents handled by the various pathways (Fig. 2C). Acidified nitrite, a stressor for base excision, nucleotide excision, and mismatch repair pathways (*44*, *45*), significantly reduced the growth of S cells (Fig. 2D-E). On the other hand, S cells survived better under the stress of hydrogen peroxide, an ROS agent affecting multiple DNA repair pathways (Fig. 2D-E), consistent with the elevated expression in S cells of genes involved in scavenging ROS (*30*). Bleomycin and UV light exerted significant but similar growth reduction in both P and S cells (Fig. 2D-E) suggesting that DNA break repair pathways are not likely to be altered in S cells. We infer from these results that the downregulation of mismatch repair (MMR) and base excision repair (BER) pathways are likely contributing to the higher MF of S cells.

To further identify the specific pathways whose malfunction may have produced these mutations, we focused on the eight DNA repair genes (*46*) downregulated in S cells (see Fig. 1A), and overexpressed them using clones selected from the *E. coli* ASKA ORF-eome. Only clones of *mutS*, *mutM*, and *ung* significantly reduced MFs, which were now comparable to the MF of P cells (Fig. 1E and 2F); MutS is an MMR protein, MutM is a formamidopyrimidine-DNA glycosylase and Ung is an uracil-DNA glycosylase. The latter two are involved in BER pathways (Fig. 2C).

To identify the source of the damage contributing to the high MF of S cells, we monitored intracellular nitrite and peroxide levels using commercial kits. Levels of nitrite were similar between S and P cells, while intracellular peroxide levels were elevated in S cells (Fig. 2G). Introduction of clones of known ROS catabolism genes *katE* and *sodB*, lowered the peroxide levels in S cells (Fig. 2G). These results imply that despite the increase in expression of ROS catabolism genes observed in S cells (*30*), these cells still experience ROS stress.

In summary, three lines of evidence – the nature of mutations recovered in S cells, the susceptibility of S cells to mutagens handled by MMR and BER pathways, and the elevated cellular peroxide levels in these cells, suggests that the high MF of S cells likely arises from both high cellular redox stress and decreased expression of the MMR and BER genes *mutS*, *mutM* and *ung*, which are known to handle DNA damage by ROS.

A genetic connection between efflux and DNA repair

Efflux pump expression is tightly regulated by a vast network of regulators (*47*). To determine if efflux and DNA repair networks (*48*) were genetically connected, we took the bottoms-up

approach summarized in Fig. 3A. The regulatory connections between genes (nodes) in these two sets of pathways were interrogated by performing a nodal analysis of the three genes uncovered in this study - *ung*, *mutS*, and *mutM* - taken from the *E. coli* MG1655 curated genetic network Ecocyc (*49*). We searched for regulatory paths connecting these three peripheral nodes to the efflux pump gene network, validating them by correlation of expression of gene-pairs using data from COLOMBOS [normalized *E. coli* gene expression data derived from 4000 experimental sets; (*50*)]; we used our RNA seq data (*30*) as an additional guide (Fig. 3B-C and fig. S3A). From all the genes participating in these regulatory paths (Fig. 3D top), only those gene pairs showing significant correlation coefficients from this analysis were considered (Fig. 3C top), and are highlighted in Fig. 3D (bottom) (see fig. S3B for paths that failed validation). The analysis revealed that downregulation of *mutS* and *ung* was controlled by *rpoS* via *sdsR* and *cpxR* nodes respectively, while downregulation of *mutM* was controlled by *crp* via *rpoH*. Therefore, *rpoS* and *crp* were the major nodes seen to connect efflux and DNA repair. RpoS is an alternative sigma factor, which controls the expression of hundreds of genes that protect the cell from stress and help survive nutrient deprivation (*51*), while CRP is a global transcription regulator of many genes mostly involved in energy metabolism (*52*).

What upstream signal might be relayed via the *rpoS* and *crp* nodes? High efflux pump activity is associated with various stress responses (*53*). Efflux consumes an enormous amount of energy [ATP, PMF or Na+/H+ antiport systems drive various pumps (*54*)] (*27, 28*). Like efflux, flagella biosynthesis and rotation during swarming also consume both PMF and ATP (*55, 56*). A high metabolic rate would be required to sustain a high PMF, which in turn would lead to high intracellular ROS. This was already inferred from gene expression data (*30*), and demonstrated experimentally as well (Fig. 2G). ROS are also produced by high cell densities (*25, 26*). Could

the two global regulators RpoS and Crp identified in our analysis likely respond to ROS stress? This hypothesis was tested by measuring the effect on MF of deleting some of the regulators identified in the nodal analysis (*rpoS* and *crp* themselves were not deleted to avoid pleotropic effects (*57*)). Deletion of the major efflux regulators *marA* and *evgA* (*54*) reduced MF, while their overexpression increased it (Fig. 3E). A double deletion of *marA* and *evgA* decreased MF of S cells almost to the level of P cells (Fig. 3E). The MarA regulon increases the expression of many efflux genes including *acrA*, *acrB*, and *tolC*. Similarly, EvgA controls the expression of efflux genes *acrD* and *mdtEF* (*54*). To test whether the effect of these regulators on MF are pleiotropic or whether they occur via the genes they are known to regulate, we overexpressed *marA* in an Δ*acrB* strain, and *evgA* in an Δ*acrD* strain; in neither case did MF increase, showing that MarA and EvgA effects are routed through their specific genetic circuits. We conclude from both the nodal analysis and the experimental data presented, that the increased activity of efflux pumps itself downregulates specific DNA repair genes.

In summary, the experiments in this section show that the global regulators RpoS and Crp link specific DNA repair genes to efflux pump regulators. The results imply that these genetic links have been integrated into a network through evolutionary forces that increase mutagenesis and hence evolvability when bacteria experience high efflux-related ROS stress – an evolutionary model similar to other widely reported modes of stress-induced mutagenesis (*58, 59*). Given that high efflux is a temporary state operative only during swarming, we suggest that the ultimate cause (*60, 61*), i.e. long-term or evolutionary importance of this reversible state is acquisition of genetic resistance.

The efflux-DNA repair network is clinically relevant to the rise in antibiotic resistance

We have shown thus far that high-efflux leads to a mutator phenotype, which in turn creates genetic resistance to antibiotics, referred to in the literature as ARM (antibiotic resistance mutations). Do these findings have any clinical significance? Mutations that increase efflux are known to provide resistance to antibiotics (*62*). However, the MF data for clinical isolates are scarce. Based on the findings in Fig. 3, we can expect to find a linkage between mutations that increase efflux and accumulation of ARMs in genomes of bacteria. To examine this, we used the Comprehensive Antibiotic Resistance Database (CARD) (*63*), which catalogues ARMs for bacteria from both clinical and non-clinical sources. We analyzed only the resistome of *E. coli* (Fig. 4A, fig. S4A-B). The data showed that the occurrence of efflux ARMs per genome follows a distribution pattern that is completely different from that of non-efflux ARMs. The fraction of genomes with efflux ARMs peaked at 17 mutations per genome and showed a gradual decrease up to 42 mutations per genome, but the fraction with non-efflux ARMs peaked at 1 mutation and started a steep decline at 4 mutations per genome (Fig. 4B). More importantly, a strong positive correlation was found between efflux ARMs vs total ARMs in a genome (Fig. 4C), supporting our hypothesis that efflux-promoting mutations tend to lead to more ARMs. Similar calculations with other categories of mutations did not show this association (Fig. 4D-F, fig. S4C-E). A Spearman correlation matrix among these categories shows efflux and total mutations to be the only significantly correlated categories (Fig. 4G, fig. S4F). These data suggest that, like in case of S cells, high efflux increases the rate of evolution of ARMs even in clinical settings, and consequently multidrug resistance.

The mutator phenotype of swarms can be inhibited by efflux pump inhibitors

The high efflux of swarm cells is further stimulated by the necrosignal AcrA, released upon death of a subpopulation (*30*). It follows that AcrA addition should increase MF. We therefore incubated both P and S cells with purified AcrA and observed a significant increase of MF in S cells, but only a modest increase in P cells (Fig. 4H). Conversely, inhibiting AcrA, which is an essential periplasmic component of the AcrA-TolC RND efflux pump, should not only reduce antibiotic outflow, but should also suppress the mutator phenotype. Using as a guide a recent study which identified several small molecules that target AcrA (*64*), we selected three compounds – Novobiocin (Nov), Clorobiocin (Clo), and NSC60339 (Fig. 4I-J) to study their effect on MF. Nov and Clo are both aminocoumarins that also target DNA gyrase activity (*65*) To circumvent this effect, we overproduced in the cells a *gyrB* mutant (R136L) conferring resistance to both Nov and Clo (*65*) (fig. S5A-C). We then treated both WT and Δ*acrA* S cells expressing $gyrB^{R136L}$ with all three inhibitors in the presence or absence of externally added AcrA. Inhibition of AcrA was observed to decrease MF for all three compounds tested (Fig. 4K-L). The increase of MF seen in WT S cells (i.e. without the *gyrB* allele) treated with Nov and Clo alone (Fig. 4K, WT columns) is consistent with the idea that antibiotics increase DNA damage from redox stress (*66*) (*28*). In contrast to Nov and Clo, the compound NSC60339 that solely targets AcrA to inhibit both efflux and necrosignaling, decreased MF even in WT. Among the three compounds tested, NSC60339 showed the best activity in decreasing both efflux- and necrosignal-mediated MF in all strain backgrounds (Fig. 4K, NSC).

In summary, we have shown that drugs targeting both efflux and AcrA reduced the MF of swarms, opening up new possibilities for interfering with evolvability to drug resistance in clinical settings. We note that a wide variety of bacteria, both Gram positive and Gram negative, show necrosignaling (*30*). In the case of *E. coli*, the necrosignal AcrA happens to be a

component of the efflux pump, making these inhibitors doubly effective. The nature of other necrosignals remains to be investigated.

A role for efflux in iron acquisition: spatial heterogeneity in efflux, redox, and cell death

Why do swarms intrinsically exhibit high efflux? Two lines of thought led us to examine whether the primary role of efflux is in obtaining iron from the environment. A variety of studies, including the finding that iron acquisition systems are upregulated, have shown that the bacteria are iron-starved on the surface (*19, 67-70*). Iron-scavenging systems encode high-affinity iron-binding siderophores, which are secreted into the extracellular matrix to bring iron back in (*71, 72*). Efflux pumps are crucial for siderophore secretion (*73, 74*). If the high efflux activity of swarmers is being employed to obtain iron as the swarm advances into new territory, center and edge zones of a swarm should differ in their amount of siderophores and free iron. Classical staining methods (*75*) to monitor siderophores could not be directly used on the swarm plate. We therefore lifted cells from different zones on swarm plates (Fig. 5A), to measure siderophores (*75*) and iron (*76*). The data are plotted as a circular bubble plot to capture the radially symmetric nature of the *E. coli* swarm (Fig. 5B-C). Siderophore levels were high at the edge and low at the center, while free iron showed a reverse trend.

If cells at the advancing edge are engaged in efflux for iron acquisition, would the edge cells experience higher ROS levels and perhaps also cell death as a consequence? Initially, ROS levels were measured in the entire swarm using the redox-sensitive biosensor roGFP, which increases its fluorescence upon oxidation of specific cysteines by ROS moieties inside the cell (*77, 78*). S cells were observed to have ~ 6-fold increase in fluorescence intensity compared to P

cells (Fig. 5D, fig. S6A). The fluorescent signal binned into two distinct sets (Fig. 5E) and was noisier (fig. S6B) than that in P cells. The frequency distribution of S cell fluorescence is shown in Fig. 5E (graph). We then isolated and measured roGFP intensity of cells separately from the center and edge of the swarm (Fig. 5F-G, fig. S6C-E). The center cells showed a single prominent peak of fluorescence indicating a homogeneous population with respect to ROS levels (Fig. 5F graph). Edge cells on the other hand were more heterogeneous and displayed two peaks (Fig. 5G graph). In addition, edge cells had ~5-fold more mean fluorescence compared to the center cells (fig. S6F).

To test whether the redox heterogeneity is a direct result of efflux activity, roGFP containing S cells were stained with Nile red, which is an indicator dye for efflux (*79*) - more Nile red accumulation indicating lower efflux. An anticorrelation between roGFP and Nile red signals was observed (Fig. 5H-J, middle and right, and fig. S6G), which followed an exponential decay (Fig. 5K). Consistent with the bimodal distribution of ROS profiles, S cells also exhibited a bi-modal distribution in efflux, which indicated the presence of two different efflux cell-types (Fig. 5I). A Nile red efflux assay confirmed that edge cells have ~40% higher efflux activity than center cells (fig. S6H). To evaluate whether cellular energetics and respiration are responsible for efflux-driven ROS stress, the redox dye 5-cyano-2,3-ditolyl tetrazolium chloride (CTC) (*80*) was used to stain the roGFP cells. Presence of CTC-formazan is a direct indicator of electron transport chain activity. There was a significant positive correlation between CTC and ROS signals (Fig. 5K-M and fig. S6G). Again, the CTC signal revealed two intensity peaks (Fig. 5L).

To test the deduction that high ROS causes more death, we treated S cells with a live-dead stain and indeed observed ~4-6-fold higher death within swarms compared to P populations

(Fig. 5N; fig. S6A). Edge cells specifically had ~3-fold higher death compared to center (Fig. 5O).

In summary, high efflux activity at the edge is likely employed for mitigating iron starvation experienced during surface growth, providing an explanation for why S cells engage in more efflux than P cells. In addition to the genetic association between high efflux and an increase in MF, ROS production from efflux itself leads to cellular damage. The data demonstrate that swarm edge and center cells are phenotypically distinct and spatially segregated with respect to efflux and death, with edge cells conducting more efflux and undergoing more death. Cell death is expected to release the necrosignal AcrA, which would further stimulate efflux, and therefore MF (Fig. 4A). A high-efflux physiology at the edge would be an added bonus while swarming in relevant habitats where the advancing edge would be expected to be at the forefront of an encounter with antibiotic-producing microbes.

Phenotype surfing: a new evolutionary model for survival of mutants in a swarm despite an increased fitness cost

Thus far, we have seen a striking segregation of various linked phenotypes – increased efflux, high ROS stress, and more cell death – at the edge of the swarm. These phenotypes are also directly correlated with high MF and with evolution of antibiotic resistance mutations. Evolution does not favor high MF because of its deleterious effects in general, especially when the population is dense (*81-84*); in fact, increasing the density of planktonic cultures actually decreases MF (*83*). So how does the swarm support high MF?

To address this enigma, we first measured the rate of evolution in swarms by applying the concept of 'evolvability' E (*85*), which is the ability of a biological system to produce phenotypic variation that is both heritable and adaptive (*86*). We defined E as a product of mutation frequency (MF) and total size of the population (N). Since N is dependent on the growth rate G of a population, we measured G for both S and P cells (fig. S7A). A 3D plot of these values showed that S cells have an unexpectedly better E than P cells, suggesting that S cells are indeed on a different evolutionary trajectory (Fig. 6A). Two observations further support this view. First, we found frequent co-occurrence of two Kan^R-conferring mutations in S isolates (Fig. 1H) in the relatively short selection window of our experiments (24-48 h), an event that is highly unlikely in P cells (*87*), where such mutants were indeed not observed. Second, majority of the Kan^R mutants (Fig. 1C-D) had reduced relative fitness (Fig. 1G).

Deleterious or neutral mutations that are normally lost by Darwinian forces, have a higher chance of becoming randomly fixed by genetic drift (*82*), which is high at the edges of an expanding population (*13*). Indeed, it has been shown that favorable mutations can become fixed at the edge via a genetic drift-based mechanism called 'gene surfing' (*13*). Using similar principles, we describe and test a 'phenotype surfing' model below, which posits that the unfavorable phenotype of high MF has an increased chance of survival at the swarm edge. Our mathematical model is described in detail in the Supplementary text (see Phenotype Surfing) and diagrammed in Fig. 6B. Here, a hypothetical favorable environment is an antibiotic zone A located at a distance f from the center (S_C) of a moving swarm (equivalent to the border in the assay schematic in Fig. 1B). A phenotypically-challenged (i.e., high MF) cell i is positioned at varying distances p from the center $S_{C.}$ For a cell exhibiting high efflux, zone A would be a favorable zone to navigate to, where it will not only survive but increase its ability to mutate. We

calculated the rate of fixation R of individuals carrying an antibiotic resistance gene, all along p. Estimation of R (see Eq 11 in 'Phenotype Surfing' Supplementary text and fig. S7B) showed that cells with high MF have decreased R near the center and increased R at the edge of the colony only in cases where MF (μ) was higher than 2 (our null hypothesis; see 'Phenotype Surfing'), in agreement with our hypothesis (Fig. 6C). To test this outcome experimentally, we measured the MFs of center and edge cells as before. The data clearly showed that edge cells have ~6-fold higher MF compared to center cells (Fig. 6D).

An important feature that separates our model from the previously described gene and genome surfing model is motility-based genetic drift (*14*). Motility would affect D indirectly because it would increase the probability of cell i reaching the swarm edge (Fig. 6D, videos S1, S2). Indeed, a significantly higher motility was observed in edge cells when compared to center cells (Fig. 6E, fig. S7C-H, and 'Aspect Ratio' in Supplementary text; see also video S3). The model is also supported by data in Fig. 1, where a majority (~70%) of the Kan^R mutants isolated from the swarm edge had secondary mutations in *dgcJ*, which specifically enhance swarming motility, implicating their improved motility in transporting Kan^R mutations to the front of the expanding swarm. That these mutations occurred within the edge population and were not simply carried there from the center, is attested to by the observation that the mutants were all unique (Fig. 1H); had they arisen earlier, one would expect to see many that inherited the exact same Kan^R-related mutation. Another line of support for the model comes from the observed heterogeneity of fitness costs associated with the Kan^R mutations (Fig. 1G, S1E, groups 1-4). The data show that mutants with low fitness survived in the swarm despite its dense nature, and were recovered at edge where a favorable selection condition was present – in this case Kanamycin.

Fig. 6F summarizes the 'phenotype surfing' model derived from the findings reported in this and other sections, and explains how an unfavorable phenotype can increase its survival frequency at the edge. The model is supported by data showing that cells in a swarm are spatially segregated with respect to phenotypes such as MF (Fig. 6D) and efflux (fig. S6H) and that motility plays a role in delivering these phenotypes to the edge. Spatial segregation of these phenotypes may be beneficial to the entire colony in two ways. First, the effective population size (*88*) of a swarm harboring individuals with high genetic relatedness is substantially high. This can support high rates of death as many individuals would still survive. Second, in case of sudden extinction events in the environment that could cause population bottlenecks (*89*), at least some of the spatially segregated individuals would have a better chance of survival. Thus, a perfect storm of events accruing at the edge creates an environment that sustains otherwise unfavorable mutations. The edge phenotype may well be applicable to biofilms if the cells here are engaged in high efflux (*90*). *B. subtilis* biofilms have been demonstrated to have a heterogeneity that includes a special edge function (*91*).

Summary

Bacterial swarms provide an excellent platform for studying both the biology and the physics of collective motion and of co-operative behavior. Moving as a dense pack bestows swarmer (S) cells with many survival advantages, but the one we focus on in this study is their temporary capacity to live through antibiotic concentrations that would be lethal if the same bacteria were growing in a planktonic (P) state. At least two swarm features help account for this capacity in *E. coli*: an altered S cell physiology that enables high drug efflux, and a mechanism to further elevate efflux upon encountering antibiotics by necrosignaling. The present study reveals several

unexpected facets of the relationship between efflux and DNA repair, of segregation of motile cells with high efflux to the edge of the swarm likely for iron acquisition, of higher cell death and resultant high mutation frequencies (MF) of edge cells. The advancing edge therefore becomes a microcosm for generation and survival of otherwise unfavorable mutations, a novel evolutionary phenomenon we have called 'phenotype surfing'.

We suggest that the initial condition that sets up the special ecology at the swarm edge is highly motile cells in the population that drive swarm expansion. These cells are also highly metabolically active because motility consumes both PMF and ATP, two energy sources that are also required for efflux. The necessity to acquire iron at the advancing edge therefore favors both phenotypes at the edge because siderophores are secreted via efflux; thus, both phenotypes are favored to expand. Upregulation of efflux brings with it a downregulation of MMR and BER pathways via a network of genetic interactions that appear to respond to the expected ROS stress in the phenotypes segregated at the edge. Dysfunction of DNA repair increases MF. In addition, ROS stress brings with it the risk of cellular damage and collateral death, leading to release of the necrosignal that further increases efflux and hence MF. Mutants that would otherwise have been lost in the interior of the swarm, circulate to the edge and survive there due to decreased competition and increased genetic drift. The positioning of the mutants at the edge provides them an opportunity for range expansion when conditions are ripe, and hence high evolvability to ARMs among other selection forces. Thus, phenotype surfing is a surprising mechanism for evolution in motile bacterial populations, which could in principle also work at the edges of biofilms. In addition to this discovery, our study also provides clues for how to interfere with high evolvability to ARMs.

Acknowledgements

We thank Jeffrey Barrick for critical comments. This work was supported by Public Health Service Grants GM118085 and AI158295 to R.M.H.

REFERENCES

1. M. F. Traxler, R. Kolter, Natural products in soil microbe interactions and evolution. *Natural product reports* **32**, 956-970 (2015); published online EpubJul (10.1039/c5np00013k).
2. L. Shallcross, N. Beckley, G. Rait, A. Hayward, I. Petersen, Antibiotic prescribing frequency amongst patients in primary care: a cohort study using electronic health records. *The Journal of antimicrobial chemotherapy* **72**, 1818-1824 (2017); published online EpubJun 1 (10.1093/jac/dkx048).
3. O. Hallatschek, P. Hersen, S. Ramanathan, D. R. Nelson, Genetic drift at expanding frontiers promotes gene segregation. *Proceedings of the National Academy of Sciences of the United States of America* **104**, 19926-19930 (2007); published online EpubDec 11 (10.1073/pnas.0710150104).
4. M. Nei, Selectionism and neutralism in molecular evolution. *Molecular biology and evolution* **22**, 2318-2342 (2005); published online EpubDec (10.1093/molbev/msi242).
5. M. A. Kohanski, D. J. Dwyer, J. J. Collins, How antibiotics kill bacteria: from targets to networks. *Nature reviews. Microbiology* **8**, 423-435 (2010); published online EpubJun (10.1038/nrmicro2333).
6. D. I. Andersson, B. R. Levin, The biological cost of antibiotic resistance. *Current opinion in microbiology* **2**, 489-493 (1999); published online EpubOct (10.1016/s1369-5274(99)00005-3).
7. E. C. Bottger, M. Pletschette, D. Andersson, Drug resistance and fitness in Mycobacterium tuberculosis infection. *The Journal of infectious diseases* **191**, 823-824; author reply 824 (2005); published online EpubMar 1 (10.1086/427517).
8. A. H. Melnyk, A. Wong, R. Kassen, The fitness costs of antibiotic resistance mutations. *Evolutionary applications* **8**, 273-283 (2015); published online EpubMar (10.1111/eva.12196).
9. J. Bjorkman, I. Nagaev, O. G. Berg, D. Hughes, D. I. Andersson, Effects of environment on compensatory mutations to ameliorate costs of antibiotic resistance. *Science* **287**, 1479-1482 (2000); published online EpubFeb 25 (10.1126/science.287.5457.1479).
10. A. Sousa, S. Magalhaes, I. Gordo, Cost of antibiotic resistance and the geometry of adaptation. *Molecular biology and evolution* **29**, 1417-1428 (2012); published online EpubMay (10.1093/molbev/msr302).
11. M. E. Hibbing, C. Fuqua, M. R. Parsek, S. B. Peterson, Bacterial competition: surviving and thriving in the microbial jungle. *Nature reviews. Microbiology* **8**, 15-25 (2010); published online EpubJan (10.1038/nrmicro2259).
12. S. P. Otto, M. C. Whitlock, The probability of fixation in populations of changing size. *Genetics* **146**, 723-733 (1997); published online EpubJun (10.1093/genetics/146.2.723).
13. O. Hallatschek, D. R. Nelson, Gene surfing in expanding populations. *Theoretical population biology* **73**, 158-170 (2008); published online EpubFeb (10.1016/j.tpb.2007.08.008).
14. M. J. Choudoir, K. Panke-Buisse, C. P. Andam, D. H. Buckley, Genome Surfing As Driver of Microbial Genomic Diversity. *Trends in microbiology* **25**, 624-636 (2017); published online EpubAug (10.1016/j.tim.2017.02.006).
15. R. M. Harshey, Bacterial motility on a surface: many ways to a common goal. *Annual review of microbiology* **57**, 249-273 (2003)10.1146/annurev.micro.57.030502.091014).
16. J. D. Partridge, R. M. Harshey, Swarming: flexible roaming plans. *Journal of bacteriology* **195**, 909-918 (2013); published online EpubMar (10.1128/JB.02063-12).
17. N. Hoiby, T. Bjarnsholt, M. Givskov, S. Molin, O. Ciofu, Antibiotic resistance of bacterial biofilms. *International journal of antimicrobial agents* **35**, 322-332 (2010); published online EpubApr (10.1016/j.ijantimicag.2009.12.011).

489 18. H. C. Flemming, J. Wingender, U. Szewzyk, P. Steinberg, S. A. Rice, S. Kjelleberg, Biofilms: an
490 emergent form of bacterial life. *Nature reviews. Microbiology* **14**, 563-575 (2016); published
491 online EpubAug 11 (10.1038/nrmicro.2016.94).
492 19. J. D. Partridge, R. M. Harshey, More than motility: Salmonella flagella contribute to overriding
493 friction and facilitating colony hydration during swarming. *Journal of bacteriology* **195**, 919-929
494 (2013); published online EpubMar (10.1128/JB.02064-12).
495 20. D. B. Kearns, A field guide to bacterial swarming motility. *Nature reviews. Microbiology* **8**, 634-
496 644 (2010); published online EpubSep (10.1038/nrmicro2405).
497 21. S. Lai, J. Tremblay, E. Deziel, Swarming motility: a multicellular behaviour conferring
498 antimicrobial resistance. *Environmental microbiology* **11**, 126-136 (2009); published online
499 EpubJan (10.1111/j.1462-2920.2008.01747.x).
500 22. M. T. Butler, Q. Wang, R. M. Harshey, Cell density and mobility protect swarming bacteria
501 against antibiotics. *Proceedings of the National Academy of Sciences of the United States of*
502 *America* **107**, 3776-3781 (2010); published online EpubFeb 23 (10.1073/pnas.0910934107).
503 23. W. Kim, T. Killam, V. Sood, M. G. Surette, Swarm-cell differentiation in Salmonella enterica
504 serovar typhimurium results in elevated resistance to multiple antibiotics. *Journal of*
505 *bacteriology* **185**, 3111-3117 (2003); published online EpubMay (
506 24. A. Brauner, O. Fridman, O. Gefen, N. Q. Balaban, Distinguishing between resistance, tolerance
507 and persistence to antibiotic treatment. *Nature reviews. Microbiology* **14**, 320-330 (2016);
508 published online EpubApr (10.1038/nrmicro.2016.34).
509 25. D. E. Chang, D. J. Smalley, T. Conway, Gene expression profiling of Escherichia coli growth
510 transitions: an expanded stringent response model. *Molecular microbiology* **45**, 289-306 (2002);
511 published online EpubJul (10.1046/j.1365-2958.2002.03001.x).
512 26. S. Dukan, T. Nystrom, Bacterial senescence: stasis results in increased and differential oxidation
513 of cytoplasmic proteins leading to developmental induction of the heat shock regulon. *Genes &*
514 *development* **12**, 3431-3441 (1998); published online EpubNov 1 (10.1101/gad.12.21.3431).
515 27. F. C. Fang, Antimicrobial actions of reactive oxygen species. *mBio* **2**,
516 (2011)10.1128/mBio.00141-11).
517 28. J. A. Imlay, The molecular mechanisms and physiological consequences of oxidative stress:
518 lessons from a model bacterium. *Nature reviews. Microbiology* **11**, 443-454 (2013); published
519 online EpubJul (10.1038/nrmicro3032).
520 29. J. Anes, M. P. McCusker, S. Fanning, M. Martins, The ins and outs of RND efflux pumps in
521 Escherichia coli. *Frontiers in microbiology* **6**, 587 (2015)10.3389/fmicb.2015.00587).
522 30. S. Bhattacharyya, D. M. Walker, R. M. Harshey, Dead cells release a 'necrosignal' that activates
523 antibiotic survival pathways in bacterial swarms. *Nature communications* **11**, 4157 (2020);
524 published online EpubAug 19 (10.1038/s41467-020-17709-0).
525 31. I. El Meouche, M. J. Dunlop, Heterogeneity in efflux pump expression predisposes antibiotic-
526 resistant cells to mutation. *Science* **362**, 686-690 (2018); published online EpubNov 9
527 (10.1126/science.aar7981).
528 32. J. H. Miller, D. Ganem, P. Lu, A. Schmitz, Genetic studies of the lac repressor. I. Correlation of
529 mutational sites with specific amino acid residues: construction of a colinear gene-protein map.
530 *Journal of molecular biology* **109**, 275-298 (1977); published online EpubJan 15 (10.1016/s0022-
531 2836(77)80034-x).
532 33. R. G. Fowler, J. A. Erickson, R. J. Isbell, Activity of the Escherichia coli mutT mutator allele in an
533 anaerobic environment. *Journal of bacteriology* **176**, 7727-7729 (1994); published online
534 EpubDec (10.1128/jb.176.24.7727-7729.1994).

535 34. I. Kapoor, E. A. F. Emam, A. Shaw, U. Varshney, Nucleoside Diphosphate Kinase Escalates A-to-C
536 Mutations in MutT-Deficient Strains of Escherichia coli. *Journal of bacteriology* **202**, (2019);
537 published online EpubDec 6 (10.1128/JB.00567-19).
538 35. R. M. Voorhees, V. Ramakrishnan, Structural basis of the translational elongation cycle. *Annual*
539 *review of biochemistry* **82**, 203-236 (2013)10.1146/annurev-biochem-113009-092313).
540 36. F. J. Hol, B. Hubert, C. Dekker, J. E. Keymer, Density-dependent adaptive resistance allows
541 swimming bacteria to colonize an antibiotic gradient. *The ISME journal* **10**, 30-38 (2016);
542 published online EpubJan (10.1038/ismej.2015.107).
543 37. B. Becker, M. A. Cooper, Aminoglycoside antibiotics in the 21st century. *ACS chemical biology* **8**,
544 105-115 (2013); published online EpubJan 18 (10.1021/cb3005116).
545 38. U. Jenal, A. Reinders, C. Lori, Cyclic di-GMP: second messenger extraordinaire. *Nature reviews.*
546 *Microbiology* **15**, 271-284 (2017); published online EpubMay (10.1038/nrmicro.2016.190).
547 39. C. Pesavento, G. Becker, N. Sommerfeldt, A. Possling, N. Tschowri, A. Mehlis, R. Hengge, Inverse
548 regulatory coordination of motility and curli-mediated adhesion in Escherichia coli. *Genes &*
549 *development* **22**, 2434-2446 (2008); published online EpubSep 1 (10.1101/gad.475808).
550 40. J. Zhou, L. Lancaster, J. P. Donohue, H. F. Noller, How the ribosome hands the A-site tRNA to the
551 P site during EF-G-catalyzed translocation. *Science* **345**, 1188-1191 (2014); published online
552 EpubSep 5 (10.1126/science.1255030).
553 41. S. R. Connell, C. Takemoto, D. N. Wilson, H. Wang, K. Murayama, T. Terada, M. Shirouzu, M.
554 Rost, M. Schuler, J. Giesebrecht, M. Dabrowski, T. Mielke, P. Fucini, S. Yokoyama, C. M. Spahn,
555 Structural basis for interaction of the ribosome with the switch regions of GTP-bound elongation
556 factors. *Molecular cell* **25**, 751-764 (2007); published online EpubMar 9
557 (10.1016/j.molcel.2007.01.027).
558 42. K. R. Allison, M. P. Brynildsen, J. J. Collins, Metabolite-enabled eradication of bacterial persisters
559 by aminoglycosides. *Nature* **473**, 216-220 (2011); published online EpubMay 12
560 (10.1038/nature10069).
561 43. R. Hengge, Principles of c-di-GMP signalling in bacteria. *Nature reviews. Microbiology* **7**, 263-273
562 (2009); published online EpubApr (10.1038/nrmicro2109).
563 44. B. W. Davies, R. W. Bogard, N. M. Dupes, T. A. Gerstenfeld, L. A. Simmons, J. J. Mekalanos, DNA
564 damage and reactive nitrogen species are barriers to Vibrio cholerae colonization of the infant
565 mouse intestine. *PLoS pathogens* **7**, e1001295 (2011); published online EpubFeb
566 (10.1371/journal.ppat.1001295).
567 45. K. Kurthkoti, P. Kumar, R. Jain, U. Varshney, Important role of the nucleotide excision repair
568 pathway in Mycobacterium smegmatis in conferring protection against commonly encountered
569 DNA-damaging agents. *Microbiology* **154**, 2776-2785 (2008); published online EpubSep
570 (10.1099/mic.0.2008/019638-0).
571 46. E. C. F. E. C. Friedberg, *DNA repair and mutagenesis*. (ASM Press, Washington, D.C., 2006).
572 47. J. Sun, Z. Deng, A. Yan, Bacterial multidrug efflux pumps: mechanisms, physiology and
573 pharmacological exploitations. *Biochemical and biophysical research communications* **453**, 254-
574 267 (2014); published online EpubOct 17 (10.1016/j.bbrc.2014.05.090).
575 48. K. Milanowska, J. Krwawicz, G. Papaj, J. Kosinski, K. Poleszak, J. Lesiak, E. Osinska, K. Rother, J. M.
576 Bujnicki, REPAIRtoire--a database of DNA repair pathways. *Nucleic acids research* **39**, D788-792
577 (2011); published online EpubJan (10.1093/nar/gkq1087).
578 49. I. M. Keseler, J. Collado-Vides, A. Santos-Zavaleta, M. Peralta-Gil, S. Gama-Castro, L. Muniz-
579 Rascado, C. Bonavides-Martinez, S. Paley, M. Krummenacker, T. Altman, P. Kaipa, A. Spaulding, J.
580 Pacheco, M. Latendresse, C. Fulcher, M. Sarker, A. G. Shearer, A. Mackie, I. Paulsen, R. P.
581 Gunsalus, P. D. Karp, EcoCyc: a comprehensive database of Escherichia coli biology. *Nucleic acids*
582 *research* **39**, D583-590 (2011); published online EpubJan (10.1093/nar/gkq1143).

583 50. M. Moretto, P. Sonego, N. Dierckxsens, M. Brilli, L. Bianco, D. Ledezma-Tejeida, S. Gama-Castro,
584 M. Galardini, C. Romualdi, K. Laukens, J. Collado-Vides, P. Meysman, K. Engelen, COLOMBOS
585 v3.0: leveraging gene expression compendia for cross-species analyses. *Nucleic acids research*
586 **44**, D620-623 (2016); published online EpubJan 4 (10.1093/nar/gkv1251).
587 51. P. Landini, T. Egli, J. Wolf, S. Lacour, sigmaS, a major player in the response to environmental
588 stresses in Escherichia coli: role, regulation and mechanisms of promoter recognition.
589 *Environmental microbiology reports* **6**, 1-13 (2014); published online EpubFeb (10.1111/1758-
590 2229.12112).
591 52. D. C. Grainger, D. Hurd, M. Harrison, J. Holdstock, S. J. Busby, Studies of the distribution of
592 Escherichia coli cAMP-receptor protein and RNA polymerase along the E. coli chromosome.
593 *Proceedings of the National Academy of Sciences of the United States of America* **102**, 17693-
594 17698 (2005); published online EpubDec 6 (10.1073/pnas.0506687102).
595 53. J. L. Rosner, R. G. Martin, Reduction of cellular stress by TolC-dependent efflux pumps in
596 Escherichia coli indicated by BaeSR and CpxARP activation of spy in efflux mutants. *Journal of*
597 *bacteriology* **195**, 1042-1050 (2013); published online EpubMar (10.1128/JB.01996-12).
598 54. D. Du, X. Wang-Kan, A. Neuberger, H. W. van Veen, K. M. Pos, L. J. V. Piddock, B. F. Luisi,
599 Multidrug efflux pumps: structure, function and regulation. *Nature reviews. Microbiology* **16**,
600 523-539 (2018); published online EpubSep (10.1038/s41579-018-0048-6).
601 55. F. F. Chevance, K. T. Hughes, Coordinating assembly of a bacterial macromolecular machine.
602 *Nature reviews. Microbiology* **6**, 455-465 (2008); published online EpubJun
603 (10.1038/nrmicro1887).
604 56. C. V. Gabel, H. C. Berg, The speed of the flagellar rotary motor of Escherichia coli varies linearly
605 with protonmotive force. *Proceedings of the National Academy of Sciences of the United States*
606 *of America* **100**, 8748-8751 (2003); published online EpubJul 22 (10.1073/pnas.1533395100).
607 57. A. Ishihama, T. Shimada, Y. Yamazaki, Transcription profile of Escherichia coli: genomic SELEX
608 search for regulatory targets of transcription factors. *Nucleic acids research* **44**, 2058-2074
609 (2016); published online EpubMar 18 (10.1093/nar/gkw051).
610 58. R. C. MacLean, C. Torres-Barcelo, R. Moxon, Evaluating evolutionary models of stress-induced
611 mutagenesis in bacteria. *Nature reviews. Genetics* **14**, 221-227 (2013); published online
612 EpubMar (10.1038/nrg3415).
613 59. Y. Ram, L. Hadany, Stress-induced mutagenesis and complex adaptation. *Proceedings. Biological*
614 *sciences* **281**, (2014); published online EpubOct 7 (10.1098/rspb.2014.1025).
615 60. K. N. Laland, K. Sterelny, J. Odling-Smee, W. Hoppitt, T. Uller, Cause and effect in biology
616 revisited: is Mayr's proximate-ultimate dichotomy still useful? *Science* **334**, 1512-1516 (2011);
617 published online EpubDec 16 (10.1126/science.1210879).
618 61. E. Mayr, Cause and effect in biology. *Science* **134**, 1501-1506 (1961); published online EpubNov
619 10 (10.1126/science.134.3489.1501).
620 62. X. Z. Li, P. Plesiat, H. Nikaido, The challenge of efflux-mediated antibiotic resistance in Gram-
621 negative bacteria. *Clinical microbiology reviews* **28**, 337-418 (2015); published online EpubApr
622 (10.1128/CMR.00117-14).
623 63. B. P. Alcock, A. R. Raphenya, T. T. Y. Lau, K. K. Tsang, M. Bouchard, A. Edalatmand, W. Huynh, A.
624 V. Nguyen, A. A. Cheng, S. Liu, S. Y. Min, A. Miroshnichenko, H. K. Tran, R. E. Werfalli, J. A. Nasir,
625 M. Oloni, D. J. Speicher, A. Florescu, B. Singh, M. Faltyn, A. Hernandez-Koutoucheva, A. N.
626 Sharma, E. Bordeleau, A. C. Pawlowski, H. L. Zubyk, D. Dooley, E. Griffiths, F. Maguire, G. L.
627 Winsor, R. G. Beiko, F. S. L. Brinkman, W. W. L. Hsiao, G. V. Domselaar, A. G. McArthur, CARD
628 2020: antibiotic resistome surveillance with the comprehensive antibiotic resistance database.
629 *Nucleic acids research* **48**, D517-D525 (2020); published online EpubJan 8 (10.1093/nar/gkz935).

630 64. N. Abdali, J. M. Parks, K. M. Haynes, J. L. Chaney, A. T. Green, D. Wolloscheck, J. K. Walker, V. V.
631 Rybenkov, J. Baudry, J. C. Smith, H. I. Zgurskaya, Reviving Antibiotics: Efflux Pump Inhibitors That
632 Interact with AcrA, a Membrane Fusion Protein of the AcrAB-TolC Multidrug Efflux Pump. *ACS*
633 *infectious diseases* **3**, 89-98 (2017); published online EpubJan 13 (10.1021/acsinfecdis.6b00167).
634 65. C. H. Gross, J. D. Parsons, T. H. Grossman, P. S. Charifson, S. Bellon, J. Jernee, M. Dwyer, S. P.
635 Chambers, W. Markland, M. Botfield, S. A. Raybuck, Active-site residues of Escherichia coli DNA
636 gyrase required in coupling ATP hydrolysis to DNA supercoiling and amino acid substitutions
637 leading to novobiocin resistance. *Antimicrobial agents and chemotherapy* **47**, 1037-1046 (2003);
638 published online EpubMar (10.1128/AAC.47.3.1037-1046.2003).
639 66. D. J. Dwyer, P. A. Belenky, J. H. Yang, I. C. MacDonald, J. D. Martell, N. Takahashi, C. T. Chan, M.
640 A. Lobritz, D. Braff, E. G. Schwarz, J. D. Ye, M. Pati, M. Vercruysse, P. S. Ralifo, K. R. Allison, A. S.
641 Khalil, A. Y. Ting, G. C. Walker, J. J. Collins, Antibiotics induce redox-related physiological
642 alterations as part of their lethality. *Proceedings of the National Academy of Sciences of the*
643 *United States of America* **111**, E2100-2109 (2014); published online EpubMay 20
644 (10.1073/pnas.1401876111).
645 67. T. Inoue, R. Shingaki, S. Hirose, K. Waki, H. Mori, K. Fukui, Genome-wide screening of genes
646 required for swarming motility in Escherichia coli K-12. *Journal of bacteriology* **189**, 950-957
647 (2007); published online EpubFeb (10.1128/JB.01294-06).
648 68. Q. Wang, J. G. Frye, M. McClelland, R. M. Harshey, Gene expression patterns during swarming in
649 Salmonella typhimurium: genes specific to surface growth and putative new motility and
650 pathogenicity genes. *Molecular microbiology* **52**, 169-187 (2004); published online EpubApr
651 (10.1111/j.1365-2958.2003.03977.x).
652 69. C. S. Lin, Y. H. Tsai, C. J. Chang, S. F. Tseng, T. R. Wu, C. C. Lu, T. S. Wu, J. J. Lu, J. T. Horng, J.
653 Martel, D. M. Ojcius, H. C. Lai, J. D. Young, An iron detection system determines bacterial
654 swarming initiation and biofilm formation. *Scientific reports* **6**, 36747 (2016); published online
655 EpubNov 15 (10.1038/srep36747).
656 70. L. McCarter, M. Silverman, Iron regulation of swarmer cell differentiation of Vibrio
657 parahaemolyticus. *Journal of bacteriology* **171**, 731-736 (1989); published online EpubFeb
658 (10.1128/jb.171.2.731-736.1989).
659 71. B. R. Wilson, A. R. Bogdan, M. Miyazawa, K. Hashimoto, Y. Tsuji, Siderophores in Iron
660 Metabolism: From Mechanism to Therapy Potential. *Trends in molecular medicine* **22**, 1077-
661 1090 (2016); published online EpubDec (10.1016/j.molmed.2016.10.005).
662 72. J. Kramer, O. Ozkaya, R. Kummerli, Bacterial siderophores in community and host interactions.
663 *Nature reviews. Microbiology* **18**, 152-163 (2020); published online EpubMar (10.1038/s41579-
664 019-0284-4).
665 73. C. Bleuel, C. Grosse, N. Taudte, J. Scherer, D. Wesenberg, G. J. Krauss, D. H. Nies, G. Grass, TolC is
666 involved in enterobactin efflux across the outer membrane of Escherichia coli. *Journal of*
667 *bacteriology* **187**, 6701-6707 (2005); published online EpubOct (10.1128/JB.187.19.6701-
668 6707.2005).
669 74. P. J. F. Henderson, C. Maher, L. D. H. Elbourne, B. A. Eijkelkamp, I. T. Paulsen, K. A. Hassan,
670 Physiological Functions of Bacterial "Multidrug" Efflux Pumps. *Chemical reviews* **121**, 5417-5478
671 (2021); published online EpubMay 12 (10.1021/acs.chemrev.0c01226).
672 75. B. Schwyn, J. B. Neilands, Universal chemical assay for the detection and determination of
673 siderophores. *Analytical biochemistry* **160**, 47-56 (1987); published online EpubJan
674 (10.1016/0003-2697(87)90612-9).
675 76. C. Oviedo, D. Contreras, J. Freer, J. Rodriguez, A screening method for detecting iron reducing
676 wood-rot fungi. *Biotechnology letters* **25**, 891-893 (2003); published online EpubJun
677 (10.1023/a:1024086524974).

678 77. B. Morgan, M. C. Sobotta, T. P. Dick, Measuring E(GSH) and H2O2 with roGFP2-based redox
679 probes. *Free radical biology & medicine* **51**, 1943-1951 (2011); published online EpubDec 1
680 (10.1016/j.freeradbiomed.2011.08.035).
681 78. J. van der Heijden, S. L. Vogt, L. A. Reynolds, J. Pena-Diaz, A. Tupin, L. Aussel, B. B. Finlay,
682 Exploring the redox balance inside gram-negative bacteria with redox-sensitive GFP. *Free radical*
683 *biology & medicine* **91**, 34-44 (2016); published online EpubFeb
684 (10.1016/j.freeradbiomed.2015.11.029).
685 79. J. A. Bohnert, B. Karamian, H. Nikaido, Optimized Nile Red efflux assay of AcrAB-TolC multidrug
686 efflux system shows competition between substrates. *Antimicrobial agents and chemotherapy*
687 **54**, 3770-3775 (2010); published online EpubSep (10.1128/AAC.00620-10).
688 80. G. G. Rodriguez, D. Phipps, K. Ishiguro, H. F. Ridgway, Use of a fluorescent redox probe for direct
689 visualization of actively respiring bacteria. *Applied and environmental microbiology* **58**, 1801-
690 1808 (1992); published online EpubJun (10.1128/aem.58.6.1801-1808.1992).
691 81. K. Sprouffske, J. Aguilar-Rodriguez, P. Sniegowski, A. Wagner, High mutation rates limit
692 evolutionary adaptation in Escherichia coli. *PLoS genetics* **14**, e1007324 (2018); published online
693 EpubApr (10.1371/journal.pgen.1007324).
694 82. M. Lynch, M. S. Ackerman, J. F. Gout, H. Long, W. Sung, W. K. Thomas, P. L. Foster, Genetic drift,
695 selection and the evolution of the mutation rate. *Nature reviews. Genetics* **17**, 704-714 (2016);
696 published online EpubOct 14 (10.1038/nrg.2016.104).
697 83. R. Krasovec, R. V. Belavkin, J. A. Aston, A. Channon, E. Aston, B. M. Rash, M. Kadirvel, S. Forbes,
698 C. G. Knight, Mutation rate plasticity in rifampicin resistance depends on Escherichia coli cell-cell
699 interactions. *Nature communications* **5**, 3742 (2014); published online EpubApr 29
700 (10.1038/ncomms4742).
701 84. R. Krasovec, H. Richards, D. R. Gifford, C. Hatcher, K. J. Faulkner, R. V. Belavkin, A. Channon, E.
702 Aston, A. J. McBain, C. G. Knight, Spontaneous mutation rate is a plastic trait associated with
703 population density across domains of life. *PLoS biology* **15**, e2002731 (2017); published online
704 EpubAug (10.1371/journal.pbio.2002731).
705 85. M. Pigliucci, Is evolvability evolvable? *Nature reviews. Genetics* **9**, 75-82 (2008); published online
706 EpubJan (10.1038/nrg2278).
707 86. J. L. Payne, A. Wagner, The causes of evolvability and their evolution. *Nature reviews. Genetics*
708 **20**, 24-38 (2019); published online EpubJan (10.1038/s41576-018-0069-z).
709 87. S. F. Elena, R. E. Lenski, Evolution experiments with microorganisms: the dynamics and genetic
710 bases of adaptation. *Nature reviews. Genetics* **4**, 457-469 (2003); published online EpubJun
711 (10.1038/nrg1088).
712 88. M. Husemann, F. E. Zachos, R. J. Paxton, J. C. Habel, Effective population size in ecology and
713 evolution. *Heredity* **117**, 191-192 (2016); published online EpubOct (10.1038/hdy.2016.75).
714 89. E. Libby, P. B. Rainey, Exclusion rules, bottlenecks and the evolution of stochastic phenotype
715 switching. *Proceedings. Biological sciences* **278**, 3574-3583 (2011); published online EpubDec 7
716 (10.1098/rspb.2011.0146).
717 90. I. Alav, J. M. Sutton, K. M. Rahman, Role of bacterial efflux pumps in biofilm formation. *The*
718 *Journal of antimicrobial chemotherapy* **73**, 2003-2020 (2018); published online EpubAug 1
719 (10.1093/jac/dky042).
720 91. J. W. Larkin, X. Zhai, K. Kikuchi, S. E. Redford, A. Prindle, J. Liu, S. Greenfield, A. M. Walczak, J.
721 Garcia-Ojalvo, A. Mugler, G. M. Suel, Signal Percolation within a Bacterial Community. *Cell*
722 *systems* **7**, 137-145 e133 (2018); published online EpubAug 22 (10.1016/j.cels.2018.06.005).

723

Fig. 1

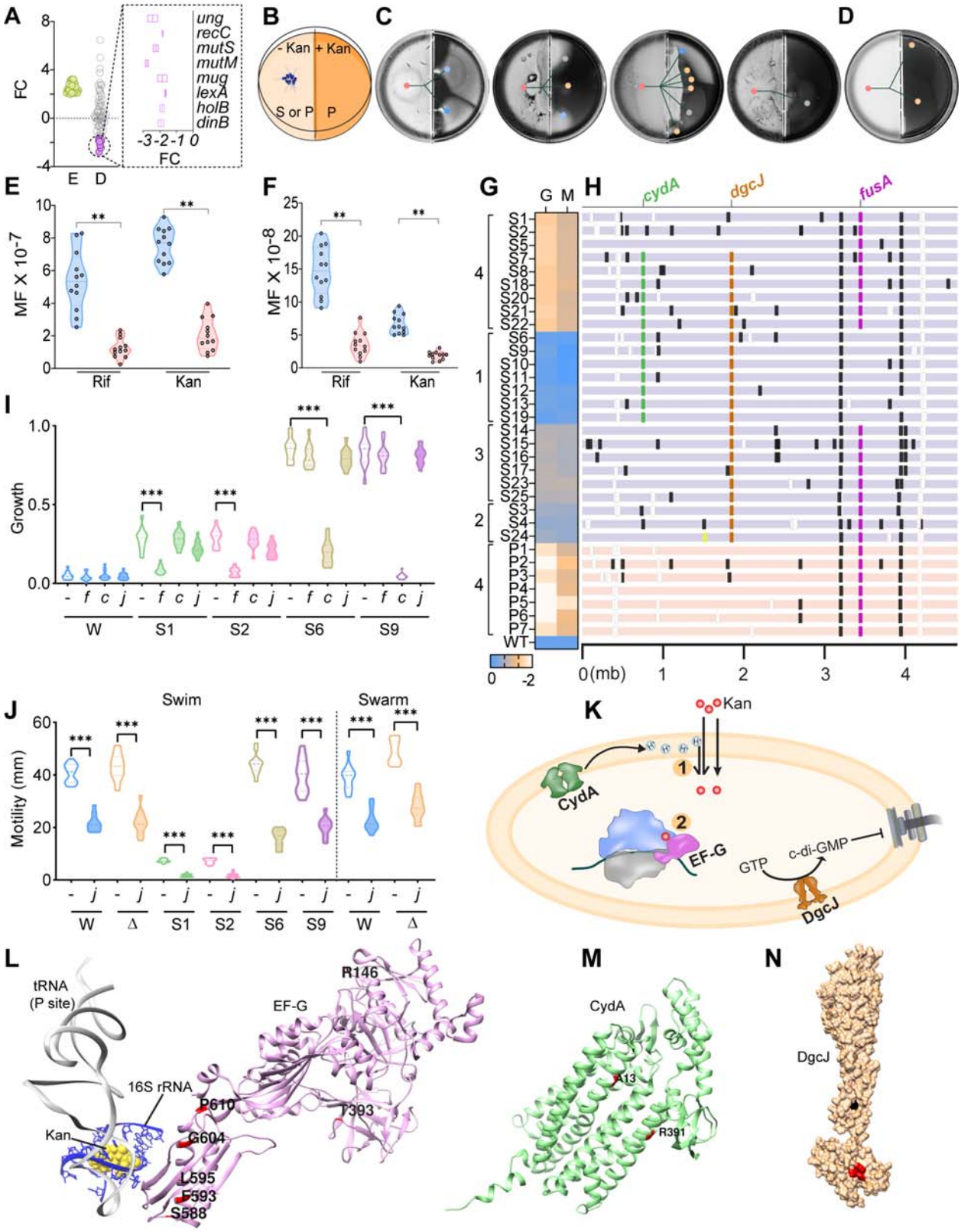
A
FC
ung
recC
mutS
mutM
mug
lexA
holB
dinB
-3 -2 -1 0
FC
E D
B
- Kan + Kan
S or P
P
C
D
E
MF X 10^-7
Rif
Kan
F
MF X 10^-8
Rif
Kan
G
G M
H
cydA
dgcJ
fusA
S1
S2
S4
S5
S7
S8
S18
S20
S21
S22
S6
S9
S10
S11
S12
S13
S19
S14
S15
S16
S17
S23
S25
S3
S4
S24
P1
P2
P3
P4
P5
P6
P7
WT
0 -2
0(mb) 1 2 3 4
I
Growth
W S1 S2 S6 S9
J
Swim
Swarm
Motility (mm)
W Δ S1 S2 S6 S9 W Δ
K
Kan
CydA
EF-G
GTP
c-di-GMP
DgcJ
L
tRNA
(P site)
EF-G
R146
16S rRNA
P610
T393
Kan
G604
L595
F593
S588
M
CydA
A13
R391
N
DgcJ

724

Fig. 1. Swarms downregulate DNA repair and show high evolvability to antibiotic resistance

(A) Log2-fold change (FC) in expression of efflux and DNA-repair genes in *E. coli* swarm cells. Inset: DNA-repair genes downregulated more than 1.5 log2-fold.

(B) Border-crossing assay schematic. S: swarm, P: swim; Kan = 25u/ml Kanamycin or Kan^{25}. Bacteria are inoculated in the left no-Kan chamber.

(C-D) WT *E. coli* inoculated on the left on either swarm (C) or swim (D) media, crossed the border into Kan^{25} swim media. Representative plates show the emergence of Kan-resistant (Kan^{R}) swimmers. Color-coded circles mark distinct phenotypes (see H): Lines between circles indicate the lineage of mutants from WT.

(E-F) Mutation frequencies (MF) of S (blue) and P (red) cells of (E) *E. coli* and (F) *B. subtilis*, measured by resistance to Rifampicin (Rif^{50}) and Kan^{50}. Each black circle is an experimental replicate. [$^{**}p < 0.01$, Mann-Whitney test]

(G) Heat map showing the growth G, and motility M, of Kan^{R} mutants from C-D, compared to WT. S1-25 were derived from C and P1-7 from D. The clusters of isolated mutants are indicated as 1-4 matching mutant color codes from (C-D)).

(H) Summary of mutations from the individual isolates listed in G scaled to the *E. coli* genome in Mb (bottom). Syntenic mutations in the 3 indicated genes were recovered frequently. White and black boxes = inter- or intragenic mutations.

(I-J) Comparison of growth (I) of indicated mutant and WT strains in Kan^{25} media, and motility (J) in swim media. *f, c, g* indicates complementation with plasmids expressing *fusA*, *cydA*, *dgcJ*; Δ, Δ*dgcJ*. [$^{***}p < 0.001$, Wilcoxon rank sum test]

(K) A schematic summarizing possible effects of recovered mutations in *fusA*, *cydA*, *dgcJ*. (1) *cydA* mutations reduce PMF which may decrease Kan uptake. (2) *fusA* mutations reverse the translation inhibition by Kan. *dgcJ* mutations are expected to reduce c-di-GMP and increase motility.

(L-N) Structures of (L) EF-G (*fusA*; magenta) [PDB:4V7D], (M) CydA [PDB:6RKO], and (N) DgcJ [Alphafold]. Red: active site mutations; black: other mutations. In each gene, multiple mutations from different S-P isolates map to the same site.

Fig. 2

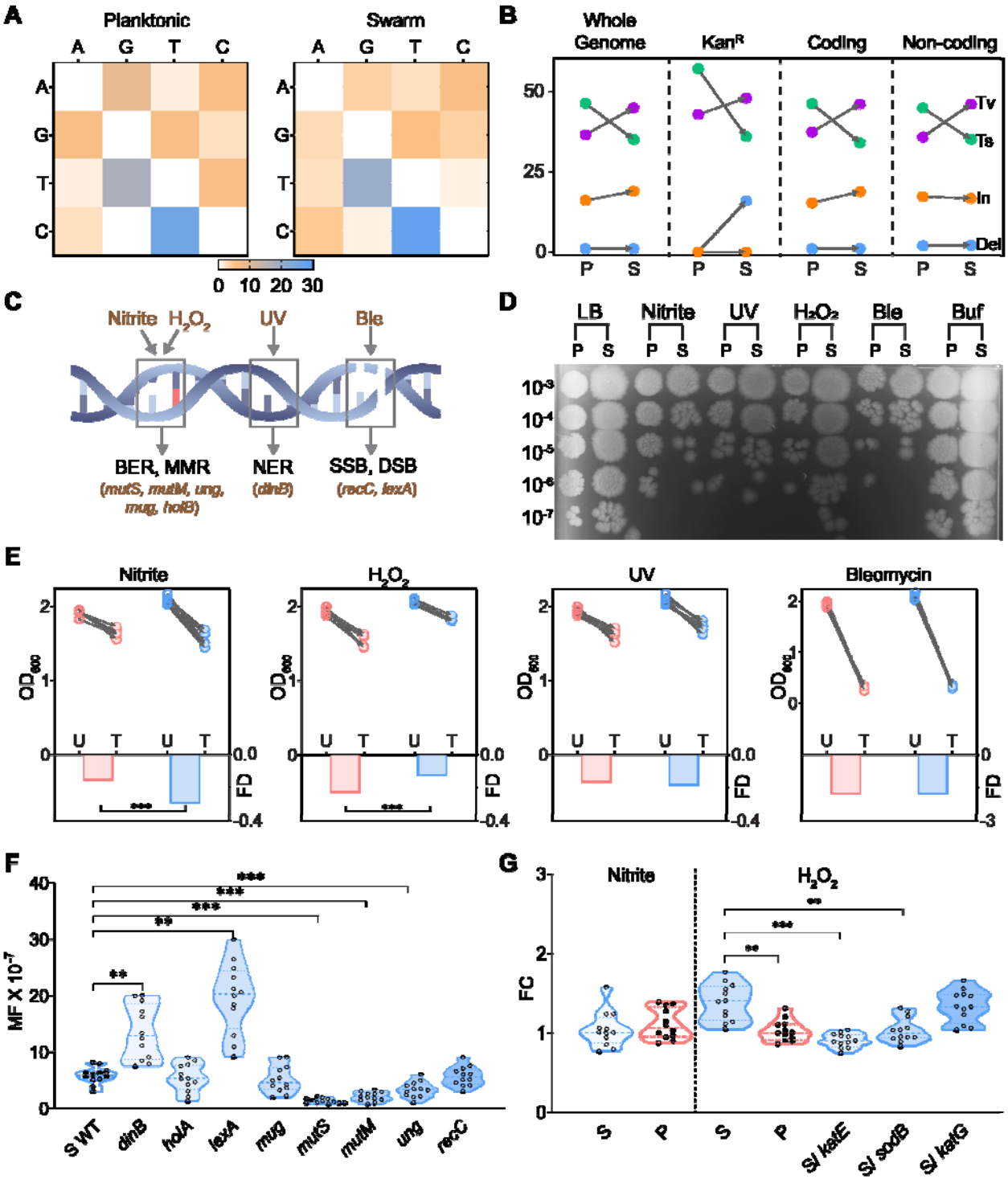

Fig. 2. Downregulation of mismatch and base excision repair pathways contributes to the higher MFs of swarm cells

(A) Heatmaps showing percentages of different types of mutations found in P and S mutants. WT nucleotides are on the left column, and rows show mutations in P1-P7 and S1-S25 isolates (Fig. 1G). (B) A comparison of the percent changes (Y-axis) in types of mutations in S and P isolates. Transitions (Ts), Transversions (Tv), Insertions (In) and Deletions (Del) are color coded as indicated. All identified mutations in each group were first combined together in a set, then sorted on the basis of categories indicated on the top.

(C) Schematic showing specific DNA repair pathways and genes that primarily function in these pathways. The major types of DNA damage caused by mutagenic agents used in this study are shown on top and the pathways (and genes) for dealing with them shown at the bottom of the DNA schematic.

(D) Dilution spotting of S and P cells after treatment with: sodium nitrite (Nitrite), ultraviolet light (UV), hydrogen peroxide (H_2O_2), and bleomycin (Ble).

(E) Comparison of cell growth (OD_{600}) in the presence (T, treated) or absence (U, untreated) of indicated stresses. Blue: S, red: P. FD: mean fold-decrease in growth in T calculated as FD= log(T/U). [$^{**}p < 0.01$, paired t-tests].

(F) Rif^{50} MF of S cells measured as in Fig. 1E. WT S cells were transformed with clones of the indicated DNA repair genes and changes in MF monitored. $^{**}p < 0.01$, $^{***}p < 0.001$; Mann-Whitney test.

(G) Fold changes (FC) in Nitrite and Peroxide levels in P and S cells, measured using commercial kits. Only peroxide levels were different. *katE, sodB* and *katG* genes were overexpressed in S cells to monitor changes in these levels. $^{**}p < 0.01$, $^{***}p < 0.001$; Wilcoxon rank-sum test.

Fig. 3

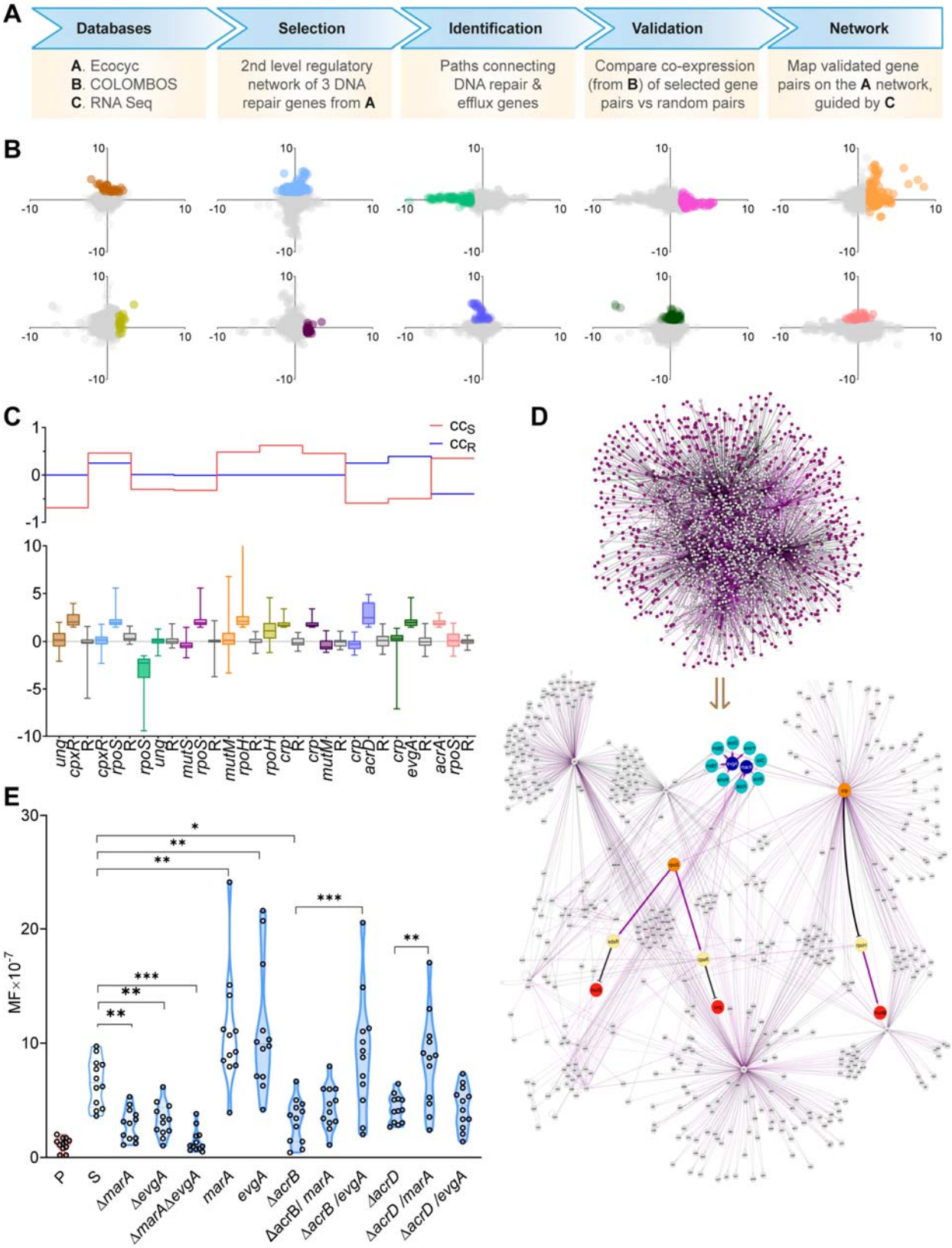
A
Databases
Selection
Identification
Validation
Network
A. Ecocyc
B. COLOMBOS
C. RNA Seq
2nd level regulatory network of 3 DNA repair genes from A
Paths connecting DNA repair & efflux genes
Compare co-expression (from B) of selected gene pairs vs random pairs
Map validated gene pairs on the A network, guided by C
B
C
CCS
CCR
D
E
MF×10-7
P
S
ΔmarA
ΔevgA
ΔmarAΔevgA
marA
evgA
ΔacrB
ΔacrB/ marA
ΔacrB /evgA
ΔacrD
ΔacrD /marA
ΔacrD /evgA

784

Fig. 3. A genetic connection between efflux and DNA repair

(A) Flowchart summarizing the network analysis performed in this study.

(B) Scatterplots showing expression of different gene-pairs within the network that connect efflux genes with DNA repair genes (color-coded as the gene-pairs in (C)); significant fold changes (± 1.5) are shown in matching colors with (C).

(C) Bottom: Boxplot showing distribution of significant changes color-coded in B; R is one of 100 randomized pairs (see fig. S3A). Top: Lines indicating the calculated Pearson correlation coefficients (CC) of the corresponding pairs at the bottom. CC_S, selected pair; CC_R, random pair.

(D) Top: Connection of 2nd level regulatory network of DNA repair genes *mutS*, *mutM* and *ung* to efflux genes, selected from the 1st level whole network (from database A in Fig. 3A). Purple: terminal nodes; Grey: connecting nodes. Bottom: Validated portion of network from Top, with genetic connections between efflux (cyan) and DNA repair (red) genes. The connectors are efflux regulators (navy), major regulators of repair genes (orange), and genes connecting regulators with DNA repair (yellow). Dashed blue lines indicate an effect of efflux activity on regulators. Flatheads, downregulation; Arrows, upregulation.

(E) Rif^{50} MF analysis of P (red) and S (blue) cells. X axis lists genetic background of S cells. [$*p < 0.05$, $**p < 0.01$, $***p < 0.001$; Mann-Whitney test]

Fig. 4

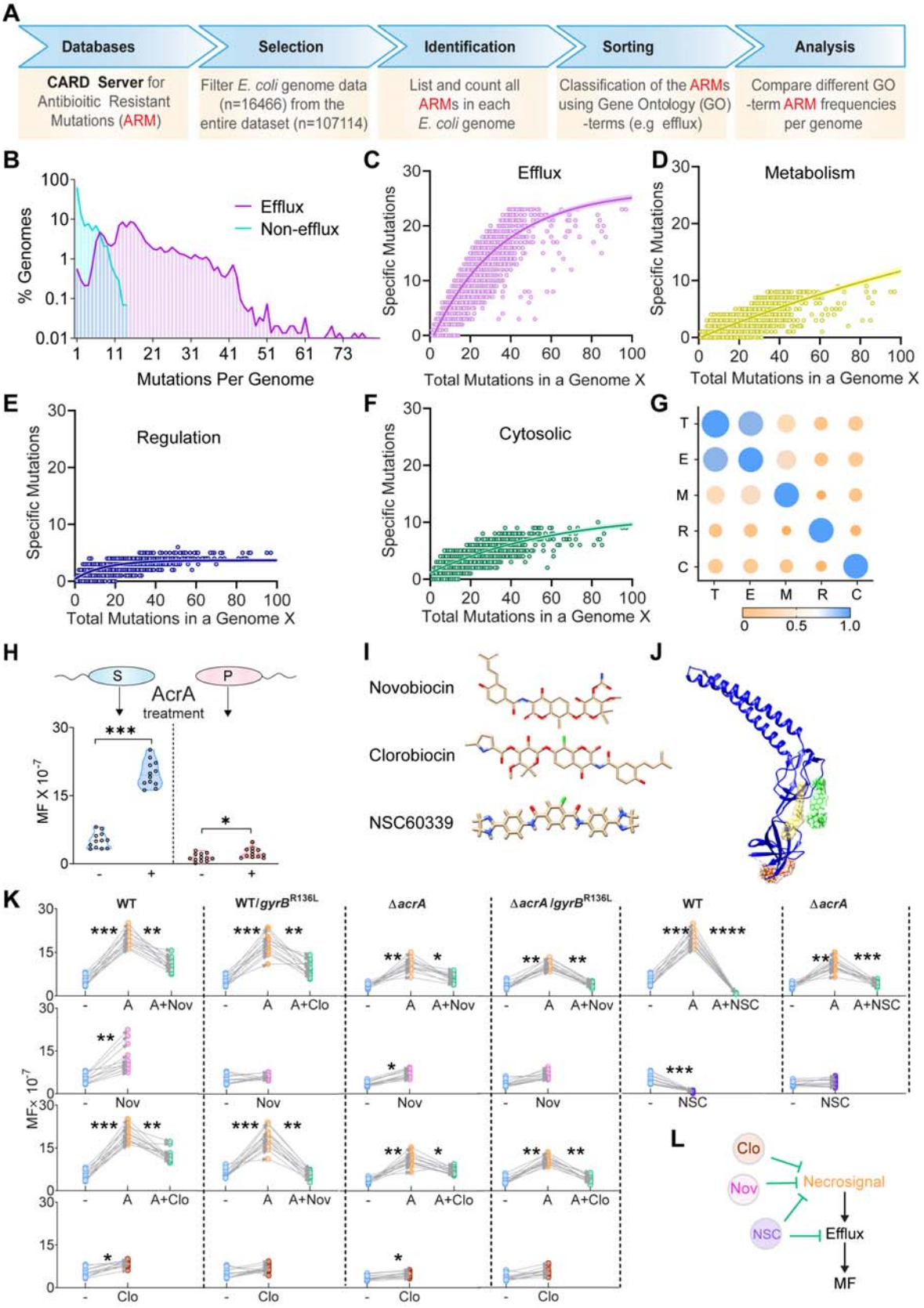
A
Databases
Selection
Identification
Sorting
Analysis
CARD Server for Antibioitic Resistant Mutations (ARM)
Filter E. coli genome data (n=16466) from the entire dataset (n=107114)
List and count all ARMs in each E. coli genome
Classification of the ARMs using Gene Ontology (GO) -terms (e.g efflux)
Compare different GO -term ARM frequencies per genome
B
% Genomes
Efflux
Non-efflux
Mutations Per Genome
C
Efflux
Specific Mutations
Total Mutations in a Genome X
D
Metabolism
Specific Mutations
Total Mutations in a Genome X
E
Regulation
Specific Mutations
Total Mutations in a Genome X
F
Cytosolic
Specific Mutations
Total Mutations in a Genome X
G
T
E
M
R
C
0
0.5
1.0
H
S
P
AcrA
treatment
MF X 10^-7
I
Novobiocin
Clorobiocin
NSC60339
J
K
WT
WT/gyrB^R136L
ΔacrA
ΔacrA/gyrB^R136L
WT
ΔacrA
A
A+Nov
A+Clo
A+NSC
Nov
NSC
Clo
MF× 10^-7
L
Clo
Nov
NSC
Necrosignal
Efflux
MF

802

Fig. 4. The efflux-DNA repair network is clinically relevant to the rise in antibiotic resistance which can be inhibited by efflux pump inhibitors

(A) Flowchart summarizing the analysis of the *E. coli* antibiotic resistome data from CARD.

(B-G) Results from the analysis in (A). (B) Frequency distributions of mutations per genome in efflux and non-efflux genomes. (C-F) Scatter plots of total number of mutations in a given genome X vs number of ARMs in a specific category of genes (indicated on top) in that genome. One category from each parent GO (Gene Ontology) class was taken for comparison (see fig. S4A-B for details). (G) Bubble matrix of calculated Spearman correlation coefficients using the data in (C). T: total; E: Efflux; M: metabolism; R: regulatory; and C: cytosolic.

(H) Top; experimental design of MF analysis. Bottom; Kan^{50} MF of S (blue) and P (red) treated (+) or untreated (-) with AcrA. [*$p < 0.05$, ***$p < 0.001$, Mann-Whitney test]

(I) Potential efflux pump inhibitors.

(J) Interaction of inhibitors in I with AcrA (PDB:2F1M).

(K) Rif^{50} MFs of WT and Δ*acrA* strains (S cells) with or without the $gyrB^{R136L}$ allele in the presence of necrosignal AcrA and indicated inhibitors. -, no additions; Nov, Novobiocin; Clo, Clorobiocin; NSC, NSC60339; A, purified AcrA. *$p < 0.05$, **$p < 0.01$, ***$p < 0.001$, ****$p < 0.0001$; Mann-Whitney test.

(L) Schematic summarizing the results in K.

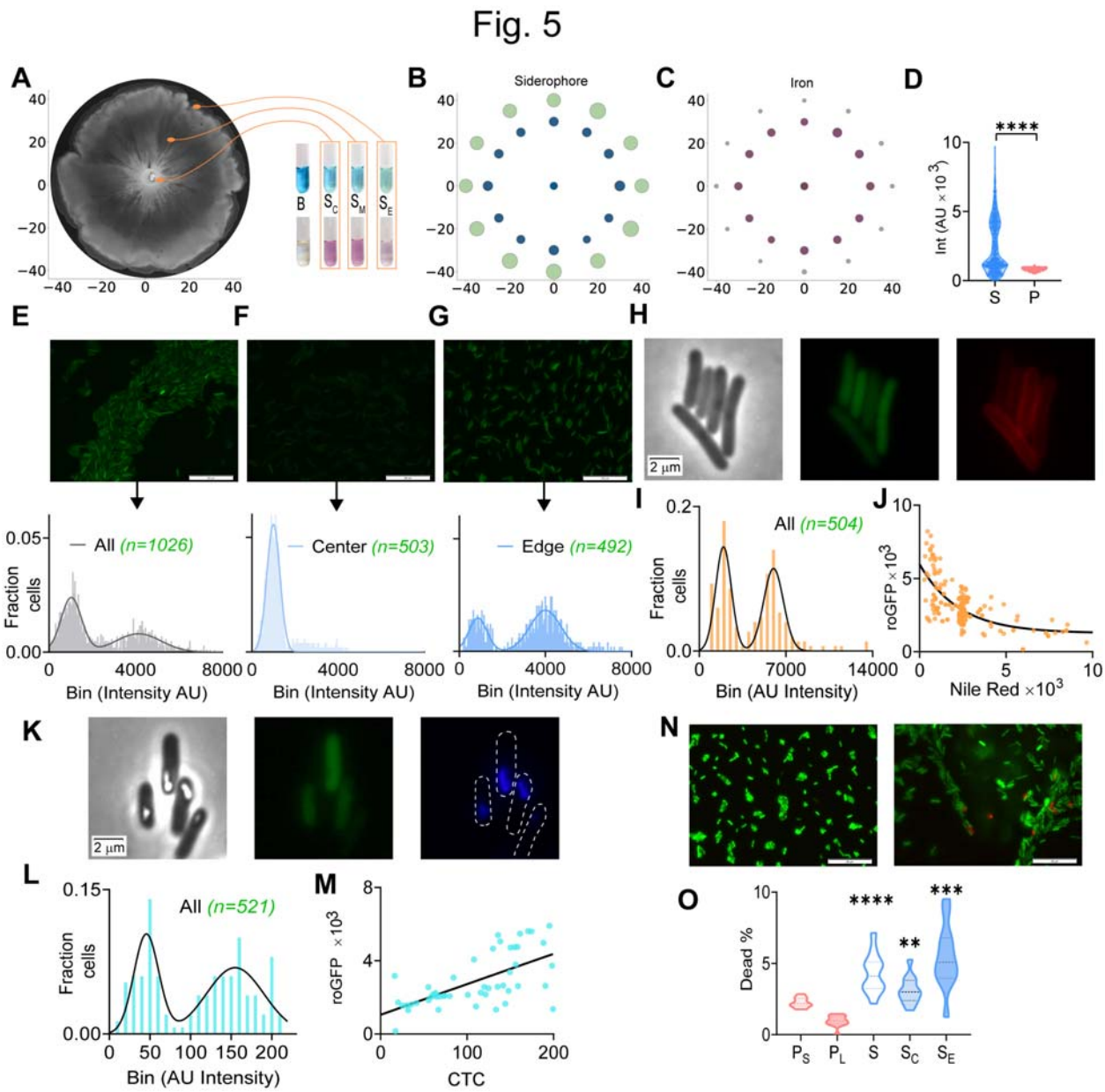

Fig. 5. A role for efflux in iron acquisition: spatial heterogeneity in efflux, redox, and cell death

(A-C) Measurement of iron in swarm cells. (A) Positioning of a swarm plate on a X-Y axis with -45 to 45 mm on each direction from center. Cells from three separate regions were collected, (S_C: center, S_M: middle, S_E: edge, B: blank reagent). (B) Siderophore (blue tubes in A, O-CAS assay) and (C) Iron concentration (magenta tubes in A, ferrozine assay) measurements at the edge and center normalized to the mean of center values. In the circular bubble-plot along the X-Y axis of the plate, each bubble represents one replicate at the indicated locations on the plate. Bubble size and color corresponds to the measured fold-change and color intensity in the assays.

(D) Quantification of roGFP intensities in S (n=1026) and P (n=792) cells (see Fig. 5E, and fig. S6A for S and P cell data); ****$p < 0.0001$; Wilcoxon rank-sum test.

(E-G) roGFP fluorescence images (top) and frequency distribution (bottom) of S cells collected from the entire swarm plate. (E) Two populations of fluorescence intensities are observed (AU, arbitrary units) (see fig. S6 C-E for brightfield images). (F, G) as in E except S cells were taken from either the center or the edge.

(H-J) roGFP-efflux correlation in S cells. (H) From left to right: bright field, roGFP, Nile red dye. (I) Distribution of Nile red fluorescence. (J) Anti-correlation of Nile red and roGFP (n=202); R^2= 0.5919.

(K-M) roGFP-CTC correlation in S cells. (K) From left to right: bright field, roGFP, CTC (false colored blue). (L) Distribution of CTC fluorescence. (M) Correlation of CTC and roGFP (n=51); R^2= 0.5012.

(N) Live-Dead staining of P (left) and S (right) cells showing superimposed live (SYTO9) and dead (PI) stains (see fig. S5I for brightfield images).

(O) percentage of dead cells. P_S, P stationary; P_L, P log phase; S_C and S_E, S cells from center and edge of swarm (see D). [t-tests performed by comparing each S set to P_S, **$p < 0.01$, ***$p < 0.001$, ****$p < 0.0001$]

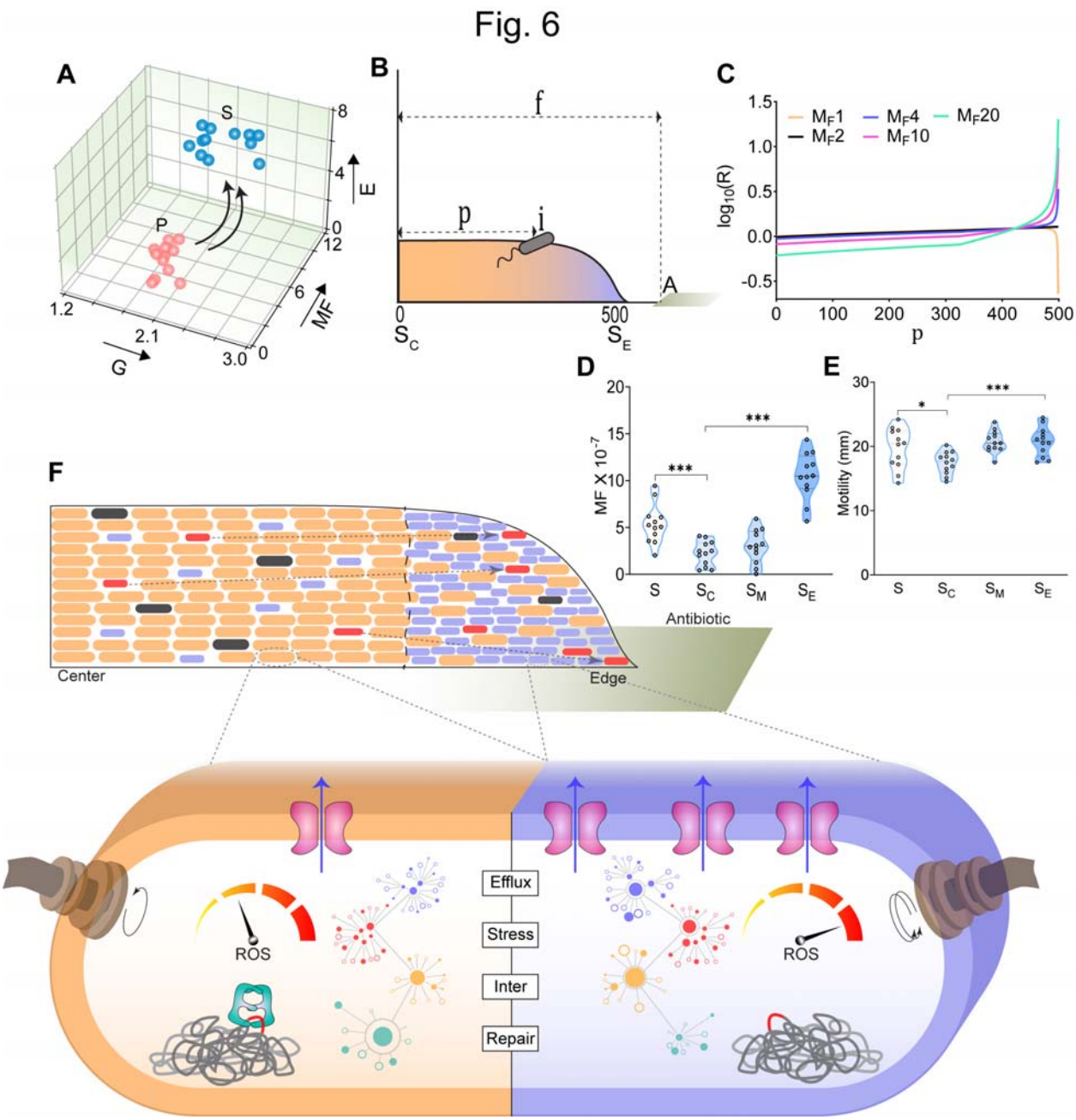

Fig. 6. A 'phenotype surfing' model explains survival in a swarm despite an increased fitness cost

(A) A 3D plot of experimentally derived values of growth rate (G, in generations per hour, x-axis), mutation frequency (MF in 10^{-7}/CFU, y-axis), and evolvability (E, Z-axis). Arrows indicate direction of change.

(B-C) A mathematical model explaining phenotypic surfing. (D) Schematic of the hypothetical situation considered in the model. Side view of a swarm (S_C: center, S_E: edge) with a radial length of 500 μm, in which a phenotypically-challenged (i.e., high μ) cell 'i' positioned at a distance 'p' from the center. An antibiotic zone 'A' which is favorable for the cell 'i' (olive) is

located at a distance ‘f’ from S_C. (E) Rate of resistance ‘R’ for each ‘p’ distance unit calculated for different mutation frequencies (M_F, $1\times10^{-7} \leq \mu \leq 20 \times10^{-7}$).

(D) Rif^{50} MF of S cells sampled from different regions. S refers to entire population.

(E) Swim motility assays with cells collected from swarm plates.

(F) Phenotypic surfing model. Top: a side view of a swarm population with the distribution of two phenotypically distinct cell types (orange and blue) in a spatially segregated edge zone. In this example, the edge has reached an antibiotic zone (olive). Blue cells are more motile and efflux more, producing mutants (red and black) some of which die (black) in absence of a favorable environment. The blue cells and their red progeny ‘surf’ at the edge of the colony either by a faster migration to the edge (dashed arrows) or are favored at the edge to bring in iron. Bottom: Summary of mechanism underlying the phenotypic differences between orange and blue cells. The yellow-red gauge indicates ROS levels, which are high in blue cells. A series of network interactions starting from efflux nodes (blue), through stress (red), and other intermediate nodes (Inter, yellow) decrease DNA repair activity (teal) in blue cells, increasing mutations (red).

(D-E) $*p < 0.05$, $***p < 0.001$; Mann-Whitney test.